PRIFYSGOL
BANGOR
UNIVERSITY

A standardised tidal-stream power curve, optimised for the global resource

Lewis, Matthew; O'Hara Murray, Rory; Fredriksson, Sam; Maskell, John; de Fockert, Anton; Neill, Simon; Robins, Peter

Renewable Energy

Peer reviewed version

Cyswllt i'r cyhoeddiad / Link to publication

13. Mar. 2024

Journal Pre-proof

A standardised tidal-stream power curve, optimised for the global resource

Matt Lewis, Rory O'Hara Murray, Sam Fredriksson, John Maskell, Anton de Fockert, Simon Neill, Peter Robins
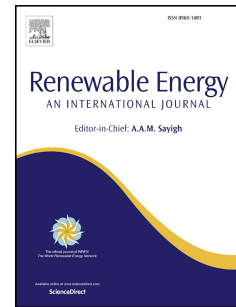
Please cite this article as: Lewis M, O'Hara Murray R, Fredriksson S, Maskell J, de Fockert A, Neill S, Robins P, A standardised tidal-stream power curve, optimised for the global resource, *Renewable Energy*, https://doi.org/10.1016/j.renene.2021.02.032.

This is a PDF file of an article that has undergone enhancements after acceptance, such as the addition of a cover page and metadata, and formatting for readability, but it is not yet the definitive version of record. This version will undergo additional copyediting, typesetting and review before it is published in its final form, but we are providing this version to give early visibility of the article. Please note that, during the production process, errors may be discovered which could affect the content, and all legal disclaimers that apply to the journal pertain.

1 **Title: A standardised tidal-stream power curve, optimised for the global resource**
2

3 Matt Lewis[1*], Rory O'Hara Murray [2], Sam Fredriksson[3] John Maskell[4], Anton de Fockert[5],
4 Simon Neill[1] , Peter Robins[1]
5

6 [1] School of Ocean Sciences, Bangor University, UK;
7 [2] Marine Scotland Science, The Scottish Government, UK;
8 [3] University of Gothenburg, Sweden; Swedish Meteorological and Hydrological Institute,
9 [4]JM Coastal Ltd,
10 [5]Deltares, Delft, NL
11

12 **Abstract**
13 Tidal-stream energy can be predicted deterministically, provided tidal harmonics and turbine-
14 device characteristics are known. Many turbine designs exist, all having different
15 characteristics (e.g. rated speed), which creates uncertainty in resource assessment or
16 renewable energy system-design decision-making. A standardised normalised tidal-stream
17 power-density curve was parameterised with data from 14 operational horizontal-axis
18 turbines (e.g. mean cut-in speed was ~30% of rated speed). Applying FES2014 global tidal
19 data (1/16° gridded resolution) up to 25 km from the coast, allowed optimal turbine rated
20 speed assessment. Maximum yield was found for turbine rated speed ~97% of maximum
21 current speed (maxU) using the 4 largest tidal constituents (M2, S2, K1 and O1) and ~87%
22 maxU for a "high yield" scenario (highest Capacity Factor in top 5% of yield cases); with little
23 spatial variability found for either. Optimisation for firm power (highest Capacity Factor with
24 power gaps less than 2 hours), which is important for problematic or expensive energy-
25 storage cases (e.g. off-grid), turbine rated speed of ~56% maxU was found – but with spatial
26 variability due to tidal form and maximum current speed. We find optimisation and
27 convergent design is possible, and our standardised power curve should help future
28 research in resource and environmental impact assessment.
29

30 **Keywords: tidal-stream energy; power curve; resource; optimization; renewable**
31 **energy**
32

33   **1. Introduction**
34 Tidal energy can be extracted using hydrokinetic devices or "in-stream" tidal-stream energy
35 converters (e.g. Tsai and Chen, 2014; Masters et al., 2015), based on the principle that
36 power (P) is a function of the cube of the volumetrically averaged current velocity (u) over
37 the rotor swept area (A), turbine power coefficient (Cp) and seawater density (ρ):
38 $P = \frac{1}{2} \rho \, Cp \, A \, u^3$ [1].
39

40 As nations look to increase their renewable energy capacity in response to climate change
41 (Neill et al., 2016) or improve access to affordable electricity (Goward-Brown, et al., 2019;
42 Zhang et al., 2019), tidal-stream energy could offer one substantial renewable resource due
43 to the predictability and reported power quality (Lewis et al., 2019). Three main types of tidal-
44 stream turbines are in various stages of development (for a review, see Rourke et al., 2010):
45 (1) horizontal axis turbines; (2) vertical axis turbines; and (3) rotating and reciprocating
46 devices. This paper shall focus on the horizontal axis turbine, used for the majority of test
47 and operational deployments; hence much data is available to inform and constrain our
48 analysis – such as estimation of device efficiency and the device power coefficient (Cp:
49 extracted power relative to the available power), alongside turbine behaviour parameters
50 including turbine cut-in and rated speed (see Mason-Jones et al., 2012; 2013).
51

52   The potential of tidal-stream energy for a sustainable future is immense (~2.5TW M2
53 tidal energy is dissipated globally – see Egbert and Ray, 2001), with diverse applications:
54 predictable contributions of renewable electricity to a national grid (Neill et al., 2016) to

55 energy solutions for remote communities and industries (e.g. Nielsen et al., 2018), such as
56 contributing to UN sustainability goals and reducing energy poverty (e.g. Lozano and
57 Taboada, 2020). However, the costs associated with tidal energy (e.g. Vazquez and Iglesias,
58 2015) such as cost reduction through economies of scale (e.g. Johnstone et al., 2013), and
59 deployment constraints (e.g. Lewis et al., 2015), need to be reduced for the true potential of
60 tidal energy to be realised. As power is proportional to the cube of tidal current, industry has
61 predominately focused on turbines with high rated speed (>2.5m/s) at so-called "first
62 generation sites (Lewis et al., 2015). It is unclear if mass-produced lower resource tidal-
63 stream turbines for "high-value markets" could provide another route to cost reduction for the
64 industry, and the motivation for this study.
65
66 As discussed in the US Dept. Energy "Powering the Blue Economy" (LiVecchi et al.,
67 2019), there is a diverse range of potential power demands (e.g. both in size and timing of
68 power required) and higher value markets (thus economic viability). We hypothesise that
69 previous focus on MegaWatt-scale contributions from tidal-stream turbines (with high rated
70 speeds above 2.5 m/s) is creating uncertainty and may not be suitable for all potential
71 renewable energy markets (LiVecchi et al., 2019). For example, there has been a reported
72 need for power curves to aid resource mapping studies with one (1 m/s cut-in and 2.7 m/s
73 rated) predominately being applied tidal turbine design (e.g. Hardisty 2012; Vennel et al.,
74 2015; Robins et al., 2015) which may introduce bias in resource assessment (Fairley et al.,
75 2020). Furthermore, Robins et al. (2015) proposed that turbines suitable for lower flows
76 would reduce temporal variability to the resource and increase resultant net power. Tidal-
77 stream energy resource therefore appears uncertain, in part, due to uncertainty of end-user
78 power needs and device design.
79
80 Mapping the tidal resource for a region relies on validated hydrodynamic models,
81 which numerically solve versions of the Navier-Stokes equations to fully capture tidal
82 dynamics. Theoretical resource estimates for a region calculate tidal power from the ocean
83 model output variables to be applied in equation 1. Tidal resource has been shown to be
84 affected by the power extracted (e.g. Garrett and Cummins, 2005; 2007; Yang et al., 2013),
85 hence technical resource assessment often explicitly include power extraction of tidal
86 turbines to further improve potential yield estimates (e.g. Vennell et al., 2010; Goward-Brown
87 et al., 2017). Environmental impact assessments to the deployment of tidal turbines also
88 require power extraction to be explicitly resolved in the ocean model simulations; for
89 example, impacts to circulation and associated processes (e.g. Kadiri et al., 2012), sediment
90 transport pathways (Robins et al., 2014) and morphodynamics (Neill et al., 2009).
91
92 The drag force (Fd) of a tidal turbine is represented within hydrodynamic model
93 simulations applying equation 1 as:
94 $$Fd = \frac{p}{u} \ [2];$$
95 hence the impact of tidal energy conversion can be explicitly resolved in environmental
96 impact and resource assessments (see Yang et al., 2013). Tidal-stream turbine behaviour is
97 predominately based on first generation technologies (Lewis et al., 2015); where cut-in
98 speed (Vs), and rated speed (Vr: the current speed where maximum or "rated power" (Pr) is
99 extracted, with power "capped" or "shed" for current speeds above Vr) – must be resolved to
100 adequately represent turbine behaviour (e.g. Goward-Brown et al., 2017). First generation
101 tidal-stream turbines are defined by Lewis et al. (2015) as having a rated speed ~2.5 m/s,
102 and, whilst many devices indeed have high rated speeds, a number of lower flow devices
103 (e.g. Kites – see Buckland et al., 2015) and applications (O'Donncha et al., 2017) have been
104 discussed. Indeed, in many resource assessments, power curve information has been stated
105 as necessary for future work (e.g. Lewis et al., 2015; Vazquez and Iglesias, 2015; Guillou et
106 al., 2018).
107

108   The lack of data to parameterise turbine behaviour presents a significant challenge
109   due to uncertainty in the parameterisation of tidal-stream turbine behaviour. The impact of
110   various tidal turbine power curves to the technical resource assessment is shown in Figure
111   1; where a 15-day time-series of two harmonics (M2 amplitude of 2 m/s and S2 amplitude of
112   0.5 m/s) is applied to estimate theoretical power density (*P/A* using Eq. 1), and the
113   theoretical power curve of two devices: *Vr*=2.5 m/s and *Vs*=1 m/s (from Lewis et al., 2015),
114   and *Vr*=2 m/s and *Vs*=0.5 m/s (from Encarnacion et al., 2019). Although rated turbine speed
115   (*Vr*) differs by 0.5m/s between the two devices of Figure 1, with mean power and mean daily
116   energy difference of 18% and 23% respectively, the maximum drag (thus impact, estimated
117   from Eq. 2) differed by 41%. Moreover, the Capacity Factor (*CF*), defined here as the ratio of
118   energy converted relative to the maximum energy that could be converted (i.e. if at rated
119   power throughout the time-series), varied by 14% between the two devices of Figure 1; with
120   a 19% difference in the time of zero power (so called downtime) and a 2 hour difference in
121   the longest duration window of zero power output, which has implications for storage design
122   and whole system costs.
123
124
125   Given that tides are almost entirely deterministic (e.g. Lewis et al., 2019), and the
126   wide variety of potential markets globally (from large-scale power contributions to national
127   electricity distribution networks to remote "off-grid" industries and communities): are the
128   present range of tidal-stream turbine designs suitable for all global markets, and can a
129   scalable convergent solution be found? This paper aims to firstly consolidate the diverse
130   range of horizontal axis tidal turbines to a scalable power curve for unbiased resource and
131   impact assessments. The standardised power-density curve can then be applied to explore
132   convergence based on the global tidal-stream resource. We do not include the swept area in
133   our analysis as this is likely to be based on local bathymetric constraints, life cycle
134   assessment and cost optimisation. Instead our objective is to establish a method, which can
135   be applied in the future to include cost optimisation based on future markets and mass-
136   production principles (Junginger et al., 2004; Johnstone et al., 2013): providing a
137   constructive step towards a resource-led globally-optimal engineering solution for the
138   renewable energy industry.
139
140   **2. Method**
141   This study is composed of three parts: firstly, power curve data is compiled for the majority of
142   published horizontal tidal-stream turbines (i.e. all that could be found). Rated power (*Pr*) and
143   flow speed (*Vr*) allow the power coefficient (*Cp*) and thrust coefficient (*Ct*) to be estimated,
144   using variables from equations 1 and 2, because:
145    $Ct = \frac{2\,F}{\rho\,A\,u^2}$ [3];
146    $Cp = \frac{2\,P}{A\,\rho\,u^3}$ [4].
147   Consolidating the data, a normalised theoretical mean power density curve relative to rated
148   power (i.e. *P/Pr* and *u/Vr*) can be established (i.e. swept area removed), and also compared
149   to observed variability in a grid-connected tidal-stream turbine (published in Lewis et al.,
150   2019). Here, density of seawater (*ρ*) is assumed to be 1027 kg/m^3 and the turbine is
151   operated at constant Tip Speed Ratio (TSR) irrespective of swept area (*A*) or flow speed (*u*):
152   i.e. that *Cp* does not vary with flow speed and Tip Speed Ratio (Mason-Jones et al., 2012;
153   2013).
154
155   The second part of our method will apply the average power density curve
156   information (which we call the normalised power curve) to resolve optimal power curve
157   characteristics for the diverse range of potential markets and tidal energy sites globally: for
158   example, does the optimal power curve for a remote island/industry differ to an optimal tidal
159   power curve for electricity supply to a grid?
160

161   Depth averaged tidal current information was based on the FES2014 dataset (Finite
162 Element Solution data assimilated global tide model), which has a global grid resolution of
163 1/16° (Carrere et al.,, 2015). The FES2014 dataset was masked using the NASA distance-
164 to-coast dataset (resolution 1/25°) which was created using the Generic Mapping Tools
165 (GMT) coastline. Global tidal data of the four principal semi-diurnal and diurnal tidal
166 constituents (M2, S2, K1, O1), between latitudes 70°S and 70°N and included only ocean
167 grid cells that were within 25 km from land were extracted. We assume tidal energy
168 development beyond 25 km is not economically feasible based on challenges with
169 connecting to shore, and have removed tidal analysis from high latitude (>70°) due to ice
170 interaction challenges and uncertainties.

171
172   Applying the normalised power curve to a wide range of rated speeds (*Vr* discretised
173 in 0.1 m/s bins between 0.3 m/s and 6 m/s) allows power density curves for all potential
174 tidal-stream turbines to be applied to one year tidal current time-series (5 min frequency).
175 The tidal current time-series at each location was calculated using the "t_tide" toolbox: a
176 harmonic tidal prediction method, where a time-series is described from the sum of sinusoids
177 at frequencies specified from astronomical parameters (Pawlowicz et al., 2008). Global tidal
178 harmonics data were used from the FES2014 product (Carrère et al., 2015; Lyard et al.,
179 2020) for all resolved coastal locations (<25 km from land). An optimal power density curve
180 was selected for each site using three scenarios (A, A2 and B) to represent the diversity of
181 end user needs; from weighting the optimal tidal turbine power density curve based on firm
182 and constant power, or maximum possible yield. Hence, the range between high yield and
183 firm power (scenarios A and B) should therefore represent all potential optimal tidal turbine
184 solutions; providing a sensitivity test to power curve choice in resource assessment, but also
185 the potential for current technologies and concepts to be scaled for the more globally
186 prevalent, lower flow and power demand markets.

187
188 **Scenario A** (maximum yield): the power density curve that gave the highest annual energy
189 yield for each site (irrespective of storage and end user needs). We assume such a scenario
190 useful in free-market economic systems with national electricity distribution networks.

191
192 **Scenario A2** (high yield): the highest Capacity Factor (CF) for power density curves that
193 gave the top 5% of annual yields per site. Therefore, although Scenario A2 does not bound
194 the range of potential optimal tidal power curves, it is assumed to represent a likely choice
195 given other resource uncertainties (e.g. higher order tidal harmonic effects, or the impact of
196 waves (Lewis et al., 2014) and weather windows).

197
198 **Scenario B** (Firm yield): the highest yield power density curve that had a maximum gap in
199 power generation below 2 hours and consistent peak power (within 2%). We assume such a
200 firm power tidal turbine beneficial for users where likely storage potential is low, or the
201 storage costs are high (for example the use of fly wheels instead of batteries).

202
203   The third part of method aims to resolve convergence in an optimal power curve
204 based on the global tidal data; producing simplified rules for industry and researcher to
205 follow (e.g. can we assume tidal turbine rated speed to be equivalent to the peak spring tidal
206 current speed for a given site?) Finally, we investigate the impact of tidal data quality by
207 comparing our 1/16° FES2014 results to that derived from tidal harmonics calculated using a
208 much higher resolution ocean model at 1/100° (~1km instead of ~7km spatial resolution) for
209 the UK domain (14°W to 11°E, and 42°N to 62°N). Data were interpolate onto the higher
210 resolution grid and the data of the UK ROMS model details given in Robins et al. (2015).

211
212   **3. Results**
213 Horizontal-axis tidal-stream turbine power density curves were normalised and standardised
214 (Section 3.1), which can be applied to idealised tidal current time-series with increasing

215 complexity in tidal harmonics (Section 3.2), and applied to the global tidal harmonic data in
216 Section 3.3.
217
218 **3.1. Power curve analysis results**
219 Horizontal axis tidal turbine information was gathered from published data of 14 devices that
220 are in commercial development or deployment (Table 1). We believe data in Table 1 to be
221 the most comprehensive, up-to-date list compiled thus far. We acknowledge that Table 1 is
222 incomplete, with some prototypes and models missing, however convergence of the
223 normalised power-density curve in Figure 2 is clear – and the addition of devices likely to
224 only impact parameters that are not considered here (e.g. swept diameter mean rated
225 power). Where key variables are missing (noted in Table 1 with *), data were extrapolated
226 using equations 1 and 4.
227
228 The rated power density and speed (Pr and Vr respectively) of the tidal-stream
229 turbines are shown in Figure 2a, compared to the theoretical (black dash line). Normalised
230 power-density curves of these devices are shown in Figure 2b, using the mean device
231 power coefficient (Cp) of Table 1, assuming Cp constant through all flow speeds, alongside
232 the measured power variability (at 0.5 Hz frequency) for a "grid connected" tidal-stream
233 turbine (taken from Lewis et al., 2019). Measured fine-scale power fluctuations of Figure 2b,
234 likely due to fine-slow flow variability and turbulence (see Lewis et al., 2019), were found to
235 be much larger than variability in mean device characteristics (cut-in and rated speed) for the
236 14 devices. Therefore Figure 2 indicates a normalised mean power curve can be used to
237 represent all horizontal axis tidal turbines currently being developed, and apply the power-
238 density curve to global tide data in Section 3.2. Finally, Figure 2a shows there is no trend in
239 diameter of the swept rotor area, especially considering the size range of turbines, shown by
240 the large standard deviation in Table 1, hence further justification to use power density in our
241 analysis - as rotor size is likely to depend on local site charactersitics and cost-benefit
242 analysis (which is beyond the scope of this work).
243
244 A standardised and normalised power curve for horizontal axis tidal-stream turbines
245 was established using the mean value of Table 1: Cut in speed of the turbine (Vs) was found
246 to be 30% of the rated speed (Vr) on average with a standard deviation (STD) of 7%, and we
247 assume power coefficient (Cp) is constant, at a mean value of 0.37; which allows the power
248 density (P/A) to be described relative to the rated power of a device (where Pr is expressed
249 as P/A relative to the rated, thus between 0% and 100%). It should be noted that the power
250 coefficient (Cp) is likely to be affected by a number of variables: flow speed and site
251 turbulence characteristics (including waves), as well as blade design and Tip-Speed-Ratio
252 (see Mason-Jones 2012; 2013) – however the variability does not significantly affect our
253 results (based on unpublished sensitivity test – varying section 3.2 with Cp with one STD:
254 0.04).
255
256 The standardised power curve, based on mean values of Table 1, is shown in Figure
257 3a and is described in equation 5, using three conditions:

$$\text{When } Vr > u > 0.3Vr: P = \frac{1}{2}\,0.37\;u^3 A\;;$$

$$\text{when } u < 0.3Vr: P = 0;$$

258 $$\text{when } u > Vr: P = Pr \quad [5].$$

259 Moreover, the normalised drag and thrust coefficient (Ct) can now also be described (using
260 Equation 2) – which allows a tidal-stream turbine, unbiased in technology choice, to be
261 represented for future resource and environmental impact assessment hydrodynamic
262 modelling methods. The device agnostic power curve of Figure 3 therefore only needs a
263 rated power (Pr) and swept area (A) to be assumed, and we shall explore an optimal Vr,
264 based on tidal resource, in Section 3.2
265
266 **3.2. Power density curve optimisation**

267   The standardised normalised power curve of Figure 3 was applied to a tidal current time-
268 series for a range of rated turbine speeds (*Vr*), with the Capacity Factor (*CF*) and the yield
269 for each theoretical device compared. Capacity Factor (*CF*) was calculated as the
270 percentage of energy captured compared to energy captured if a turbine was at rated speed
271 throughout the timeseries:

272     $CF = \frac{\int_{\frac{1}{2}} Cp\, A\, u_t^3}{\int_{\frac{1}{2}} Cp\, A\, Vr^3}$ [6]).

273

274 Here, we consider power-density in our analysis, as bathymetry likely to be uncertain in the
275 spatially coarse global data of FES2014 (1/16° see Section 3.3) and we assume swept area
276 (*A* in Eq. 1) to be controlled by cost and array-design optimisation. Furthermore, the scaling
277 of depth-averaged current (*u*) to hub-level flow is not included but cannot be represented in
278 global tide data due to sub-scale temporal and spatial variability. The swept area (*A*) can be
279 removed from our *CF* calculation (of Eq. 6), as it is a constant in the numerator and
280 denominator integral; therefore our optimisation is independent of swept area, and instead
281 our analysis focuses on the rated speed of a turbine relative to the temporal variability of the
282 tide for a given site.

283

284   The mean power density and mean daily yield (kWh/m^2 per day) were also
285 calculated as metrics of power curve performance for each theoretical power curve at each
286 site. To demonstrate the method, Figure 4 shows the optimal power density curve (Figure 3,
287 with rated turbine speeds between 0.3 m/s and 6.0 m/s in 0.1 m/s increments) for an
288 idealised tidal current, with a single M2 (principal lunar semi-diurnal tidal harmonic) of
289 amplitude 2 m/s (hence each peak current is 2 m/s with no variability between tides). The
290 optimal power curve for the simplified case of Figure 4 is a turbine with a rated speed at 2
291 m/s (as expected), with an optimal mean power and yield density of ~0.6 kW/m^2 and 15
292 kW/m^2 per day respectively (corresponding *CF* of 41%).

293   Increasing the complexity of an idealised tide example, we demonstrate the power
294 density optimisation for a site with two harmonics in Figure 5: M2 and S2 (principal solar
295 semi-diurnal harmonic), which together simulate the fortnightly "spring-neap" cycle that
296 describes 75% of UK tidal variability (Robins et al., 2015). Figure 5 demonstrates the optimal
297 power curve for an extreme case, where the S2 amplitude is 60% of the M2 signal (M2
298 amplitude = 1 m/s), such that peak current of 1.6 m/s occurs when M2 (period 12.42 hours)
299 and S2 (period 12 hours) are in-phase (spring tide), and 0.4 m/s peak current speeds occur
300 when M2 and S2 are out-of-phase (neap tide). Optimal yield for Figure 5 was found when
301 the turbine rated speed was that of the peak spring tide (*Vr*=1.6m/s) but with a much
302 reduced Capacity Factor (17%), due to the extreme nature of the M2/S2 ratio. The
303 importance of weighting the optimal tidal power curve to either yield (i.e. Scenario A or A2)
304 or consistent power (i.e. Scenario B) is demonstrated in Figure 6.

305

306   Variability in choice of an "optimal" power curve, described here as rated turbine
307 speed (Vr) relative to the M2 current amplitude (thus *Vr*/UM2), is demonstrated in Figure 6
308 for the range of M2/S2 ratios (M2/S2 of 0 has only an M2 tide, whilst equal M2 and S2
309 current amplitudes has a ratio of 1), with four metrics of turbine performance that were
310 calculated applying the idealised power density curve of Figure 3 to a rated turbine speed
311 between 0.3 m/s and 6 m/s (in steps of 0.1 m/s): hence Figure 6 is independent of resource
312 magnitude. The four metrics of turbine performance in Figure 6 were based on yield
313 performance relative to the maximum (Capacity Factor in Figure 6a and yield as a
314 percentage of the maximum possible yield Figure 6c), and the persistence of power supply:
315 percentage of time no power is produced in Figure 6b (as opposed to percentage of time at
316 rated power of Figure 6a) and the largest "power gap" where no power is produced (Figure
317 6d). The choice of what an "optimal" tidal-stream turbine is clear at the extremes of the
318 M2/S2 ratio in Figure 6, where, although extreme, a turbine with a relatively high rated speed

319 would produce large/largest yield but with a low CF and large gaps in power production (thus
320 having consequences in the design and cost of storage and power distribution).
321
322   A large number of constituents are needed to describe the complex processes which
323 give realistic tides (hour-to-hour and day-to-day variability in current speed); for example, the
324 K1 and O1 constituents together describe the diurnal inequality (one tide bigger than another
325 in a given day for semi-diurnal tidal systems), which, with the M2 and S2 constituents, can
326 describe tidal form (F value) and thus the diurnal (one tide per day), semi-diurnal (two tides
327 per day) or "mixed" nature of a tide at any site (Robins et al., 2015). The complexity of the
328 power curve optimisation, based on resource, is further developed from Figure 6 by using
329 these four principle constituents (see Figure 7). Figure 7 shows theoretical turbine
330 performance for yield (panel a) and persistent power (panel b) for all possible turbine power-
331 density curves (Vr 0.3-6 m/s) when varying an idealised tidal current based on the tidal dorm
332 (F value), calculated as the relative magnitude of diurnal and semi-diurnal principle
333 constituents (see Robins et al., 2015):
334          $F\ value = \frac{K1+O1}{M2+S2}$ [7].
335
336   Unlike Figure 6, the result of Figure 7 was found to be affected by the M2/S2 ratio as
337 multiple combinations of four constituent amplitudes can produce the same F value:
338 Therefore, the result of Figure 7 is based on a tide with a M2 amplitude of 1m/s and S2
339 amplitude being 0.1 m/s (M2/S2 = 0.1). Hence, it should be noted that the result of Figure 7
340 would be different if the F value was the same but M2/S2 ratio were different (based on
341 sensitivity test, an example of which is shown in Appendix Fig. A1). The tidal-stream power
342 density curve optimisation algorithm, which selects the rated speed (Vr) for Scenarios A, A2
343 and B (see Section 2), must therefore be explicitly resolved for each tidal energy site resolve
344 in the global data (Section 3.3). Nevertheless, the uncertainty of optimal rated speed (Vr) is
345 clear in Figure 7 as the divergence of the optimal power-density curve (described as relative
346 rated turbine speed Vr/UM2) for maximum and high yield (Scenario A and A2) or firm power
347 (red line of Scenario B) as the F value increases and the tidal dynamics change from a
348 regular semi-diurnal (F value<0.25) to a mixed (between 0.25 and 3) or diurnal (F value>3)
349 system (i.e. one tide per day tide).
350
351 **3.3. Optimal power curve analysis for the world**
352 Spatial variability of tidal dynamics are shown in Appendix A2 as details from data are not
353 clear. The variability of global tidal dynamics is shown in Figure 8 relative to resource,
354 calculated here as maximum tidal current speed (maxU) using the sum of the four major tidal
355 dynamics M2, S2, K1 and O1. Probability exceedance (Prob Exc.) of resource (maxU)
356 resolved in FES2014 data up to 25 km from a land mass is shown in Figure 8a; ~12.8% of
357 sites have maxU>1 m/s, 3.6% of sites have maxU>1.5 m/s, ~1.1% sites have maxU>2 m/s
358 and ~0.3% of global sites resolved have maxU>2.5 m/s. The majority of sites have a
359 dominant M2 current amplitude ~70% of maxU; however some potential tidal energy sites
360 (e.g. maxU>2m/s) have a much lower M2 contribution (see Figure 8b), which can also be
361 seen in Figure 8c. Grouping the tidal data of Figure 8c: 53% of sites resolved had F value
362 below 0.25 (semi-diurnal tides) and 46% were "partial" (F value between 0.25 and 3), with
363 relatively large contributions of K1 and O1 constituents. Some "high tidal resource" (e.g.
364 maxU>3 m/s) of Figure 8c exhibit F values above 3 (one tide per day), but account for ~1%
365 of the sites resolved. Figure 8 therefore indicates tidal dynamics at potential tidal-stream
366 energy sites, and thus the temporal variability of resource, will vary greatly around the world,
367 and any analysis that considers low flow sites (e.g. maxU<2.5 m/s) will have an
368 exponentially greater number of sites with varying tidal dynamics to consider (see Figure 7).
369
370   Applying the standardised power curve method (see Section 2), the optimal rated
371 turbine seed (Vr) for Scenarios A, A2 and B were computed (e.g. shown for an idealised tide
372 in Figure 7), and are shown in Figure 9. Optimal rated tidal-stream turbine speed (Vr) using

373 global data is shown in Figure 9 as absolute (Fig. 9a) and as a percentage of annual
374 maximum tidal current speed (Fig 9b). Both maximum (scenario A) and high (scenario A2)
375 optimisation solutions showed little variability with the exception of low resource sites (where
376 maximum current speed was below 1m/s), with a good linear regression fit (panel a) and
377 small standard deviation (shaded region of panel b) of Figure 9 (values given in Table 2).
378 Optimal *Vr* for Scenario B (firm power) had a large amount of variability and some trend
379 apparent with tidal resource (Table 2 and Figure 9), likely because the result was greatly
380 affected by tidal form (i.e. the relative contribution of diurnal constituents K1 and O1).

382 Annual maximum current speed (maxU) was based on the peak current speed
383 simulated at a given site in 2020 using the sum of four tidal constituent amplitudes (e.g.
384 UM2), calculated the major axis length of each tidal constituent ellipse (CMAX), i.e.
385 $maxU = UM2 + US2 + UK1 + UO1 = \sum^{m2,s2,k1,o1}(Cmax)$ [8].
386 Hence, optimal rated speed for maximum yield (Scenario A) will below 100% of maxU as this
387 rarely occurs (when the four considered constituents are in-phase). Two measures of *Vr* are
388 given (% of max U and absolute). The linear regression statistics, and discretised mean *Vr*
389 (as % of maxU) for grouped site current speeds, are given in Table 2 alongside respective
390 performance metrics of the mean trend line fit (RSQ for absolute) and Pearson correlation
391 (RHO) – associated P-value is not shown as all <0.001 at 5% significance. The standard
392 deviation (STD of Table 2) and convergence of shaded area in Figure 9b show variability in
393 an optimal rated turbine speed (relative to resource), and clear convergence can be seen in
394 the optimal yield scenarios (Scenarios A and A2).

396 Optimal rated speed (*Vr*) for scenario B (firm power) varied with resource (i.e. current
397 speed climatology at a site); with relative mean *Vr* found to increase with maximum current
398 speed (see Figure 9 and Table 2) but with a similar amount of variability (STD of Table 2).
399 This increase in scenario B relative rated turbine speed (*Vr* as % of maxU) is likely the
400 significant decrease in sites resolved when increasing maxU (see Figure 8a) as well as the
401 tendency for a semi-diurnal (Fig 8b) and dominant M2 amplitude (Fig 8c) in the tidal
402 dynamics. Furthermore, spatial variability in Scenario B was found when *Vr* (relative to
403 maxU) were grouped into 6 continents - see Table 3 and are shown in Appendix (Figure A3).
404 Therefore, our analysis shows an optimal tidal-stream turbine rated speed (*Vr*) based on firm
405 power supply – spatially varies due to the nature of the tide and the magnitude of the
406 resource.

408 **4. Discussion**
409 Complex analysis involving a large amount of data resulted in a simple set of rules
410 researchers and engineers can use in renewable energy resource assessment:
411 (1) Tidal-turbine cut-in speed (*Vs*) was found to be ~30% of rated turbine speed (*Vr*) on
412   average;
413 (2) For a deployment concerned with near-maximum yield aspirations, rated tidal-stream
414   turbine speed (*Vr*) at a given site will be ~87% to 97% of site maximum flow respectively
415   (where max flow is assumed as the sum of current speed amplitude of M2, S2, K1 and
416   O1 constituents: see Robins et al., 2015), with little global variation found;
417 (3) Deployments concerned with firm, constant power and small amounts of storage, may
418   aim to deploy tidal-stream turbines with much lower rated speeds (~56% of site maximum
419   flow), with spatial variability due to resource (maximum current speed) and the tidal form
420   (F value) – due to the nature of the tide at a given site (see Robins et al., 2015);
421 (4) Average values of normalised data from fourteen horizontal axis tidal-stream turbines
422   (Table 1), alongside our estimation of optimal cut-in and rated speed, allows a
423   standardised power curve and device behaviour (Figure 3) to be implemented in resource
424   and environmental impact assessment, without bias to one specific design (e.g. Fairley et
425   al., 2020) to allow tidal energy resource mapping for future technologies (e.g. Lewis et al.,
426   2015).

427

428   To ensure the result is not affected by the tidal harmonics data, the analysis of the
429   two scenario extremes (maximum yield and firm power: Scenarios A and B) were compared
430   to the result from tidal data at higher resolution: latitudinal resolution of 1/100°(~1 km)
431   instead of 1/16°(~7 km) in the FES2014 global data. The higher resolution tidal data was
432   taken from the Robins et al. (2015) hydrodynamic model of a UK domain (14°W to 11°E, and
433   42°N to 62°N), using the same four tidal constituents (M2, S2, K1 and O1) computed from a
434   30 day simulation. FES2014 data were interpolated to the Robins et al. (2015) computational
435   grid and domain, and *Vr* optimisation (of section 3.3) repeated; the comparison of the
436   optimisation algorithm, using tidal harmonic data from these two spatial resolutions, is shown
437   in Table 4.

438

439   To compare sensitivity of turbine optimisation to tidal model data accuracy (Table 4),
440   Root Mean Squared Error (RMSE) and Linear Regression score (RSQ) were estimated
441   assuming the higher resolution data accurate, alongside Scatter Index and the mean
442   downscaling value to convert between model spatial resolutions (e.g. M2 amplitude of
443   coarse data was 66% of the higher resolution model on average). Therefore, the tidal
444   resource data may differ between the two model resolutions (coarse data under-predicting
445   flow speed), but the optimal rated turbine design was found to be constant and independent
446   of tidal flow speed (see Table 4) likely because the relative size of the four tidal constituents,
447   used in this study, slowly spatially vary whilst tidal current magnitude is enhanced by
448   bathymetry – and thus dependant on model spatial resolution.

449

450   Indeed, the tidal data sensitivity test (Table 4) showed that although spatially coarse
451   data under-predicted tidal current speeds (both maximum and the main M2 constituent – see
452   Table 4), the optimal rated turbine speed (*Vr as a % of maxU*) was independent of tidal data
453   resolution. Anecdotal verification of optimal turbine rated speed, using the coarse data, can
454   be assessed by comparing our optimal rated speed result to an industry driven solution; for
455   example, the Meygen site (Pentland Firth) has a maximum current speed ~3.5m/s (Goward-
456   Brown et al., 2017) giving an estimated rated speed (*Vr*) of 2.9m/s to 3.4m/s (for A2 and A:
457   high to maximum yield scenarios), which is very close to the 2.65m/s to 3.05m/s turbines
458   installed at the site (e.g. Website 2) especially given the extremely coarse global tide data
459   (~7km spatial resolution).

460

461   It is likely that the relative magnitude of the major tidal constituents (i.e. excluding
462   over-tides such as M4), which describe tidal form (F value), has low spatial variability (e.g.
463   Robins et al., 2015; Lewis et al., 2017); therefore, tidal dynamics (i.e. nature of tide) are
464   resolved in coarse models as spatial variation is small, but tidal current amplitudes are
465   under-predicted because coarse models do not resolve bathymetric features that accelerate
466   tidal currents (see Lewis et al., 2015). Therefore, coarse resolution tidal data can be used to
467   resolve tidal dynamics, but not the magnitude of theoretical tidal-stream energy resource –
468   hence, future resource mapping efforts must be based on high resolution tidal data (also
469   concluded in Lewis et al., 2017). Higher tidal harmonics (such as the combination of M2 and
470   M4, leading to overtides and flood-ebb asymmetry) can have a significant effect on resource
471   assessment (Neill et al., 2014), and are enhanced by tidal-stream turbine deployments (e.g.
472   Neill et al., 2009), whilst interaction of array-scale tidal energy developments must be
473   included within resource assessment (e.g. Garrett and Cummins, 2008; Vennel et al., 2015);
474   therefore, we hope the standardised power curve presented here will lead to improved
475   understanding of tidal-stream energy potential.

476

477   The approach taken to provide a standardised power curve for use in tidal-stream
478   resource assessment, builds on the work of Hardisty (2012) in the application of an idealised
479   tidal-stream power curve, and device technology reviews of Roberts et al. (2016) and Zhou
480   et al. (2017). In the technologically mature wind energy industry (Lydia et al., 2014), there is
481   reported convergence in wind turbine cut-in speeds (due to insufficient torque to initiate

482   turbine rotation at wind speeds lower than 3m/s) and rated speeds (11-17 m/s), although
483   some variability in design depending on local wind conditions (Carrillo et al., 2013). The
484   knowledge of a common power curve in the wind industry has supported mean resource
485   assessment with much research now focusing on finer-scale variability (Trivellato et al.,
486   2012; Lydia et al., 2014). Therefore, our simple set of tidal turbine power curve rules, set out
487   in this paper, would allow improved resource and impact assessments with hydrodynamic
488   models.
489
490   Given the deterministic predictability of tidal-stream resource, and the establishment
491   of a standardised and resource-led power curve (presented here), a convergent tidal-stream
492   energy power curve should be the focus of future research to aid resource mapping (e.g.
493   "mhkit"; website 4). If we apply technology development of tidal-stream energy (based on
494   Lewis et al., 2015): 1st to 3rd generation sites have peak flow speeds >2.5m/s, 2m/s, and
495   1.5m/s respectively. Applying the high yield optimisation (Scenario A2) to the global tidal
496   data: 1st generation devices should be considered having rated speeds above 2.2 m/s (*Vs* ~
497   0.7 m/s), with 2nd generation rated speed above 1.7 m/s (*Vs* ~0.5 m/s) and 3rd generation
498   rated speed above 1.3 m/s (*Vs* ~0.4 m/s); close to the 0.5 m/s current speed threshold to
499   initiate turbine rotation (Encarnacion et al., 2019).
500
501   Technological learning has led to a reduction in the cost of wind energy devices
502   (Junginger et al., 2004), and a similar cost reduction is expected for tidal energy (Johnstone
503   et al., 2013). Our analysis confirms tidal turbine rated speed optimisation can be achieved.
504   The inclusion of swept tidal-stream turbine area, alongside economies of scale, practical and
505   socioeconomic constraints (e.g. Vazquez and Iglesias 2015), would therefore allow for a
506   convergent resource-optimised tidal turbine design and cost assessment. However, future
507   research must resolve uncertainties in array design choice (e.g. Coles et al.,, 2020); for
508   example, resolving cost of optimised device resilience (maintenance) and yield, will one
509   turbine be installed throughout a country, region or array?
510
511   The predictability of tidal energy, compared to the temporal variability of other non-
512   thermal renewable energy resources (see Lewis et al., 2019) and the analysis presented
513   here, indicates the need for develop tools that can perform "whole systems" design of
514   renewable energy systems – where the storage costs and dispatchability of power included
515   in supply-demand analysis (e.g. Stegman et al., 2017; Al Katsaprakakis et al., 2019) as well
516   as resilience and reliability (Johnstone et al., 2013). As power is proportional to the cube of
517   velocity (equation 1), challenges in competitive costed low-flow tidal turbines are clear (i.e.
518   low yields will likely raise LCOE greatly). However, the potential for low-flow tidal energy
519   devices appears great if we consider the persistence of power density achieved with a
520   Scenario B power curve (gap in power <2hours with the highest Capacity Factor), the cost of
521   storage and resilience in an off-grid energy solution: for example, Large lithium batteries
522   (~$500/kWh Nielsen et al., 2018) and the use of back-up diesel generators (e.g. Mala et al.,
523   2009).
524
525   Given the prevalence of lower tidal flow sites (e.g. Lewis et al., 2015; 2017), where
526   turbulence intensity (Lewis et al., 2019) and less mean vertical shear (Lewis et al., 2017b)
527   will improve resilience of devices (Encarnacion et al., 2019), the potential cost of low flow
528   tidal-stream turbines appears an important future step. Applying the conservative "firm
529   power" optimisation (Scenario B) to the global data: 1st generation devices would have a
530   rated speed of ~1.5 m/s (*Vs* ~0.5 m/s), 2nd generation rated speed ~1.2 m/s (*Vs* ~0.4 m/s)
531   and 3rd generation ~0.9 m/s (*Vs* ~ 0.3 m/s). Although all rated speeds in our Scenario B were
532   above the 0.5 m/s threshold, novel turbine designs are will be needed to improve tip-speed-
533   ratios of turbines at low current speed (0.5 m/s or below: Encarnacion et al., 2019). Indeed,
534   our analysis finds ~12.8% of the world's coastlines have maximum current speeds above 1
535   m/s (resolved in FES2014 up to 25km offshore and excluding high (> 70°) Latitudes), and
536   3.6% for maxU>1.5 m/s (see Figure 8 and Appendix A2); however absolute currents speeds

are known to be effected by ocean model resolution (Lewis et al., 2015; 2017) and this number is likely to be much higher. Therefore, higher resolution tidal resource data is needed to perform a full tidal-turbine device optimisation assessment, but the analysis presented here shows a suitable method once such data is available.

Previous research, using high resolution regional models, has shown less energetic flows dominate South East Asia (e.g. Encarnacion et al., 2019), such Malaysia (current velocities reaching up to 1.2 m/s Lim and Koh, 2010) and Philippines ("most areas reaching current velocities of 1.4 m/s" Encarnacion et al., 2019). The development of floating tidal-stream devices (Brown et al., 2020) has unlocked the potential for 2nd and 3rd generation tidal energy sites in the Gulf of California (where peak currents are between 1.0 and 2.4m/s, Mejia-Olivares et al., 2018), and the Kuroshio current where 1m/s to 1.5m/s oceanic currents could be harnessed with floating deep-water, large swept area devices (Liu et al., 2018). Indeed, low-flow rated (1.3 m/s to 1.7 m/s) tidal energy kites, with a large swept area, are also being tested and deployed (Buckland et al., 2015; Roberts et al., 2016). However, there is still a gap in low flow tidal turbines for lower power demand markets and "blue growth economies" (LiVecchi et al., 2019). For example, incorporation of tidal energy into offshore aquaculture would require tidal-stream devices capable of operating in <1m/s flows (see Gentry et al., 2017), and although some bio-optimisation to accelerate tidal currents is possible (O'Donncha et al., 2017) it may not be required given modest power needs (Aquatera 2014). We therefore, find two tidal-stream turbine markets and designs may be found in the future: (1) larger MegaWatt scale electricity production for grid-connected regions and (2) smaller-scale power systems that provide firm energy for higher value, remote industries and communities.

5. Conclusion

Given the sparsity of published power curves in the literature, and the diverse range of markets tidal energy could benefit, an unbiased power curve characterisation is essential to map tidal-stream energy resource. A standardised tidal-stream power curve was developed so that resource assessment beyond realised technologies can be possible. Our analysis and resource-led optimisation was unaffected by tidal data; finding divergence in rated-speed based on weighting of importance: firm power with low amounts of storage, or high yield with larger storage needs. A general rule for turbine power curve of a horizontal-axis turbine was found: cut-in speed was around 30% of the rated speed; and optimal rated speed (tidal current when peak power converted) was either ~50% or greater than 87% of a site's maximum current speed (based on sum of M2, S2, K1 and O1 harmonic constituents) for firm power or maximum yield respectively - due to the dominance of the major semi-diurnal lunar tidal constituent (M2). This paper demonstrates the "power" of deterministic predictability with tidal energy, and although temporal variability of the tidal resource appears to be captured by current tidal data products, higher resolution data could transform the tidal-stream energy industry by fully mapping the resource. This work also adds to the weight of evidence that a convergent tidal turbine design is needed, and possible, but two tidal-stream turbine types may exist: one for electricity supply to large grid connected communities, and another "lower resource" turbine for remote industry and communities that may have much lower rated speeds.

6. Acknowledgements

7. References

Al Katsaprakakis, D., Thomsen, B., Dakanali, I. and Tzirakis, K., 2019. Faroe Islands: towards 100% RES penetration. Renewable energy, 135, pp.473-484

Aquatera 2014.; Renewable power generation on aquaculture siteS, SARF093, report by Aquatera LtD, 2014, www.sarf.org.uk

Brown, S.A., Ransley, E.J., Zheng, S., Xie, N., Howey, B. and Greaves, D.M., 2020. Development of a fully nonlinear, coupled numerical model for assessment of floating tidal stream concepts. Ocean Engineering, 218, p.108253.

Buckland H, Dolerud E, Baker T. 2015. Application of Standard Tidal Performance Specification and Performance Review to a Non-Standard Tidal Energy Converter. European Wave and Tidal Energy Conference (EWTEC), Spetember 2015. Nantes, France

Carrere, L., Lyard, F., Cancet, M. and Guillot, A., 2015. FES 2014, a new tidal model on the global ocean with enhanced accuracy in shallow seas and in the Arctic region. EGU General Assembly, p. 5481.

Carrillo, C., Montaño, A.O., Cidrás, J. and Díaz-Dorado, E., 2013. Review of power curve modelling for wind turbines. Renewable and Sustainable Energy Reviews, 21, pp.572-581.

Coles, D.S., Blunden, L.S. and Bahaj, A.S., 2020. The energy yield potential of a large tidal stream turbine array in the Alderney Race. Philosophical Transactions of the Royal Society A, 378(2178), p.20190502.

Egbert, G.D. and Ray, R.D., 2001. Estimates of M2 tidal energy dissipation from TOPEX/Poseidon altimeter data. Journal of Geophysical Research: Oceans, 106(C10), pp.22475-22502.

Encarnacion, J.I., Johnstone, C. and Ordonez-Sanchez, S., 2019. Design of a horizontal axis tidal turbine for less energetic current velocity profiles. Journal of Marine Science and Engineering, 7(7), p.197.

Fairley, I., Lewis, M., Robertson, B., Hemer, M., Masters, I., Horrillo-Caraballo, J., Karunarathna, H. and Reeve, D.E., 2020. A classification system for global wave energy resources based on multivariate clustering. Applied Energy, 262, p.114515.

Garrett C, Cummins P. The efficiency of a turbine in a tidal channel. J Fluid Mech 2007;588:243e51.

Garrett C, Cummins P. The power potential of tidal currents in channels. Proc R Soc A 2005;461:2563e72. [7]

Brown, A.J.G., Neill, S.P. and Lewis, M.J., 2017. Tidal energy extraction in three-dimensional ocean models. Renewable energy, 114, pp.244-257.

Goward Brown, A.J., Lewis, M., Barton, B.I., Jeans, G. and Spall, S.A., 2019. Investigation of the Modulation of the Tidal Stream Resource by Ocean Currents through a Complex Tidal Channel. Journal of Marine Science and Engineering, 7(10), p.341.

Guillou, N., Neill, S.P. and Robins, P.E., 2018. Characterising the tidal stream power resource around France using a high-resolution harmonic database. Renewable Energy, 123, pp.706-718.

Hardisty, J., 2012. The tidal stream power curve: a case study. Energy and Power Engineering, 4(3), pp.132-136.

Johnstone, C.M., Pratt, D., Clarke, J.A. and Grant, A.D., 2013. A techno-economic analysis of tidal energy technology. Renewable Energy, 49, pp.101-106.

Junginger, M., Faaij, A. and Turkenburg, W.C., 2004. Cost reduction prospects for offshore wind farms. Wind engineering, 28(1), pp.97-118.

645 Kadiri, M., Ahmadian, R., Bockelmann-Evans, B., Rauen, W. and Falconer, R., 2012. A
646 review of the potential water quality impacts of tidal renewable energy systems.
647 Renewable and sustainable energy reviews, 16(1), pp.329-341.

648 Lewis, M., Neill, S.P., Robins, P.E. and Hashemi, M.R., 2015. Resource assessment for
649 future generations of tidal-stream energy arrays. Energy, 83, pp.403-415.

650 Lewis M, Neill S, Robins P, Goward-Brown A. 2017. A resource assessment to inform
651 second-generation tidal-stream energy device design. European Wave and Tidal
652 Energy Conference, 2017. Cork Ireland.

653 Lewis, M., Neill, S.P., Robins, P., Hashemi, M.R. and Ward, S., 2017b. Characteristics of the
654 velocity profile at tidal-stream energy sites. Renewable Energy, 114, pp.258-272.

655 Lewis, M., McNaughton, J., Márquez-Dominguez, C., Todeschini, G., Togneri, M., Masters,
656 I., Allmark, M., Stallard, T., Neill, S., Goward-Brown, A. and Robins, P., 2019. Power
657 variability of tidal-stream energy and implications for electricity supply. Energy, 183,
658 pp.1061-1074.

659 Lim, Y.S.; Koh, S.L. Analytical assessments on the potential of harnessing tidal currents for
660 electricity generation in Malaysia. Renew. Energy 2010, 35, 1024–1032

661 Liu, T.; Wang, B.; Hirose, N.; Yamashiro, T.; Yamada, H. High-resolution modeling of the
662 Kuroshio current power south of Japan. J. Ocean Eng. Mar. Energy 2018, 4, 37–55

663 LiVecchi, A., A. Copping, D. Jenne, A. Gorton, R. Preus, G. Gill, R. Robichaud, R. Green, S.
664 Geerlofs, S. Gore, D. Hume, W. McShane, C. Schmaus, H. Spence. 2019. Powering
665 the Blue Economy; Exploring Opportunities for

666 Lozano, L. and Taboada, E.B., 2020. Demystifying the authentic attributes of electricity-poor
667 populations: The electrification landscape of rural off-grid island communities in the
668 Philippines. Energy Policy, 145, p.111715.

669 Lydia, M., Kumar, S.S., Selvakumar, A.I. and Kumar, G.E.P., 2014. A comprehensive review
670 on wind turbine power curve modeling techniques. Renewable and Sustainable Energy
671 Reviews, 30, pp.452-460.

672 Lyard, F.H., Allain, D.J., Cancet, M., Carrère, L. and Picot, N., 2020. FES2014 global ocean
673 tides atlas: design and performances. Ocean Science Discussions, pp.1-40.

674 Mala, K., Schläpfer, A. and Pryor, T., 2009. Case studies of remote atoll communities in
675 Kiribati. Renewable Energy, 34(2), pp.358-361.

676 Mason-Jones, A., O'Doherty, D.M., Morris, C.E. and O'Doherty, T., 2013. Influence of a
677 velocity profile & support structure on tidal stream turbine performance. Renewable
678 Energy, 52, pp.23-30.

679 Mason-Jones, A., O'Doherty, D.M., Morris, C.E., O'Doherty, T., Byrne, C.B., Prickett, P.W.,
680 Grosvenor, R.I., Owen, I., Tedds, S. and Poole, R.J., 2012. Non-dimensional scaling of
681 tidal stream turbines. Energy, 44(1), pp.820-829.

682 Masters, I., Williams, A., Croft, T.N., Togneri, M., Edmunds, M., Zangiabadi, E., Fairley, I.
683 and Karunarathna, H., 2015. A comparison of numerical modelling techniques for tidal
684 stream turbine analysis. Energies, 8(8), pp.7833-7853.

685 Mejia-Olivares, C.J., Haigh, I.D., Wells, N.C., Coles, D.S., Lewis, M.J. and Neill, S.P., 2018.
686 Tidal-stream energy resource characterization for the Gulf of California, México.
687 Energy, 156, pp.481-491.

688 Neill, S.P., Hashemi, M.R. and Lewis, M.J., 2014. The role of tidal asymmetry in
689 characterizing the tidal energy resource of Orkney. Renewable Energy, 68, pp.337-
690 350.

691 Neill, S.P., Hashemi, M.R. and Lewis, M.J., 2016. Tidal energy leasing and tidal phasing.
692 Renewable Energy, 85, pp.580-587.

693 Neill, S.P., Litt, E.J., Couch, S.J. and Davies, A.G., 2009. The impact of tidal stream turbines
694 on large-scale sediment dynamics. Renewable Energy, 34(12), pp.2803-2812.

695 Nielsen T, McMullin D, Lenz B, Gamboa D. 2018. Toward 100% Renewables in the Faroe
696 Islands: Wind and Energy Storage Integration. 3rd Int. hybrid Power Systems
697 Workshop, Tenerife Spain, 8-9 May 2018.

O'Donncha, F., James, S.C. and Ragnoli, E., 2017. Modelling study of the effects of suspended aquaculture installations on tidal stream generation in Cobscook Bay. Renewable Energy, 102, pp.65-76.

Pawlowicz, R., Beardsley, B. and Lentz, S., 2002. Classical tidal harmonic analysis including error estimates in MATLAB using T_TIDE. Computers & Geosciences, 28(8), pp.929-937.

Polagye, B., Copping, A., Kirkendall, K., Boehlert, G., Walker, S., Wainstein, M. and Van Cleve, B., 2010. Environmental effects of tidal energy development: a scientific workshop. University of Washington, Seattle, Seattle, WA, USA, NMFS F/SPO-116, NOAA.

Roberts, A., Thomas, B., Sewell, P., Khan, Z., Balmain, S. and Gillman, J., 2016. Current tidal power technologies and their suitability for applications in coastal and marine areas. Journal of Ocean Engineering and Marine Energy, 2(2), pp.227-245.

Robins, P.E., Neill, S.P. and Lewis, M.J., 2014. Impact of tidal-stream arrays in relation to the natural variability of sedimentary processes. Renewable Energy, 72, pp.311-321.

Robins, P.E., Neill, S.P., Lewis, M.J. and Ward, S.L., 2015. Characterising the spatial and temporal variability of the tidal-stream energy resource over the northwest European shelf seas. Applied Energy, 147, pp.510-522.

Rourke, F.O., Boyle, F. and Reynolds, A., 2010. Marine current energy devices: Current status and possible future applications in Ireland. Renewable and Sustainable Energy Reviews, 14(3), pp.1026-1036.

Stegman, A., De Andres, A., Jeffrey, H., Johanning, L. and Bradley, S., 2017. Exploring Marine Energy Potential in the UK Using a Whole Systems Modelling Approach. Energies, 10(9), p.1251.

Trivellato, F., Battisti, L. and Miori, G., 2012. The ideal power curve of small wind turbines from field data. Journal of Wind Engineering and Industrial Aerodynamics, 107, pp.263-273.

Tsai, J.S. and Chen, F., 2014. The conceptual design of a tidal power plant in Taiwan. Journal of Marine Science and Engineering, 2(2), pp.506-533.

Vazquez, A. and Iglesias, G., 2015. LCOE (levelised cost of energy) mapping: a new geospatial tool for tidal stream energy. Energy, 91, pp.192-201.

Vennell R. Tuning turbines in a tidal channel. J Fluid Mech 2010;663:253e67. doi.org/10.1007/s10652-011-9214-3

Vennell, R., Funke, S.W., Draper, S., Stevens, C. and Divett, T., 2015. Designing large arrays of tidal turbines: A synthesis and review. Renewable and Sustainable Energy Reviews, 41, pp.454-472.

Website 1. Sabella published turbine characteristics. https://www.sabella.bzh/en. Accessed 2019

Website 2. Atlantis published turbine characteristics https://simecatlantis.com/. Accessed 2019.

Website 3. Schottel published turbine characteristics https://www.schottel.de/schottel-hydro/sit-instream-turbine/ Accessed 2019

Website 4. "mhkit" a toolbox for renewable energy resource assessment. https://mhkit-software.github.io/MHKiT/tidal.html Accessed 2019.

Yang, Z., Wang, T. and Copping, A.E., 2013. Modeling tidal stream energy extraction and its effects on transport processes in a tidal channel and bay system using a three-dimensional coastal ocean model. Renewable Energy, 50, pp.605-613.

Zhang, A., Sun, Y., Yang, W., Huang, H. and Feng, Y., 2019. Optimal Dispatching of Offshore Microgrid Considering Probability Prediction of Tidal Current Speed. Energies, 12(17), p.3384.

Zhou, Z.; Benbouzid, M.; Charpentier, J.F.; Sciuller, F.; Tang, T. Developments in large marine current turbine technologies—A review. Renew. Sustain. Energy Rev. 2017, 71, 852–858

8. Figure Captions:

753

754 **Fig 1. A demonstration of the effect of two tidal power curves on resource
755 assessment. A spring-neap time-series (2m/s M2 Cmax and 0.5m/s S2 Cmax) of tidal
756 current speed (panel a) is converted to theoretical power density (PD) in panel b and
757 technical power density (panel c) for a power curve rated at 2.5m/s (red line) and
758 2.0m/s (blue line).**

759

760 **Fig 2. Tidal-stream turbine characteristics from 14 commercially developed devices
761 (panel a), normalised (relative to rated power and speed) and compared to observed
762 variability (grey dots and averaged power curve in red) from a grid-connected device
763 in Lewis et al. (2019).**

764

765 **Fig 3. A standardised power curve, based on 14 horizontal axis tidal-stream turbines,
766 with the associated Drag (as percentage of maximum drag, Dr) and Thrust Coefficient
767 (CT) normalised curves.**

768

769 **Fig 4. Single harmonic tidal current (M2 amplitude 2 m/s) over a 2 day period (panel a),
770 and the theoretical power density (PD) of this current (panel b), compared to the mean
771 power density and Capacity Factor (panel c) for multiple tidal-stream turbine power
772 curves, where rated power is capped at rated speed (Vr, and cut-in speed is 30% of
773 Vr), which allows mean daily yield density to be calculated (panel d).**

774

775 **Fig 5. Spring-Neap tidal current (M2 amplitude 1 m/s, S2 amplitude 0.6 m/s) over a 7
776 day period (panel a), with the theoretical power density (PD) of this current (panel b).
777 Multiple tidal-stream turbine power curves, where rated power is capped at rated
778 speed (Vr, and cut-in speed is 30% of Vr), are applied to resolve an optimal design
779 using mean power density and Capacity Factor (panel c) and mean daily yield density
780 (panel d).**

781

782 **Fig 6. Performance of multiple tidal-stream power curves, represented here as rated
783 speed (*Vr*) relative to the resource (amplitude of M2 harmonic: *UM2*), for a given site
784 where the tidal currents are controlled solely by the spring-neap cycle and the ratio of
785 M2 and S2 amplitude (M2/S2 of 0 has only an M2 tide, whilst equal M2 and S2 current
786 amplitudes has a ratio of 1). Turbine performance is described using Capacity Factor
787 (a), percentage of time no power produced (b), (c) mean yield density (relative to
788 maximum possible) and (d) the longest period of zero power in a 15 day time-series.**

789

790 **Fig 7. Tide currents harmonic characteristic tidal form (F value), rated turbine speed
791 (relative to M2 current amplitude UM2) and subsequent yield and Capacity Factor
792 (CF) shown in panel a, with mean monthly percentage of zero power and maximum
793 period of no power (max gap) in panel b. Lines of optimal power curve shown in solid
794 white for selection of maximum yield (Scenario A), high yield (scenario A2) as dashed
795 white line and firm power (power gap < 2 h with highest CF: scenario B) as red
796 dashed line.**

797

798 **Fig 8. Global variability of tidal dynamics, described as maximum flow (maxU)
799 percentage exceedance (a) for sites "coastally" (<25 km offshore) resolved in the
800 FES2014 data, (b) coloured percentage occurrence of M2 amplitude contribution to
801 the maximum flow (as percentage of M2 current amplitude compared to maximum**

802 **current speed), and (c) coloured percentage occurrence of the tidal form (F value) that**
803 **describes the diurnal (F>3) to semi-diurnal (F<0.25) nature of the tide**
804

805 **Fig 9. Rated tidal-stream turbine speed using standardised power density curve and**
806 **three optimal solutions: Scenario A (maximum yield density shown in black), Scenario**
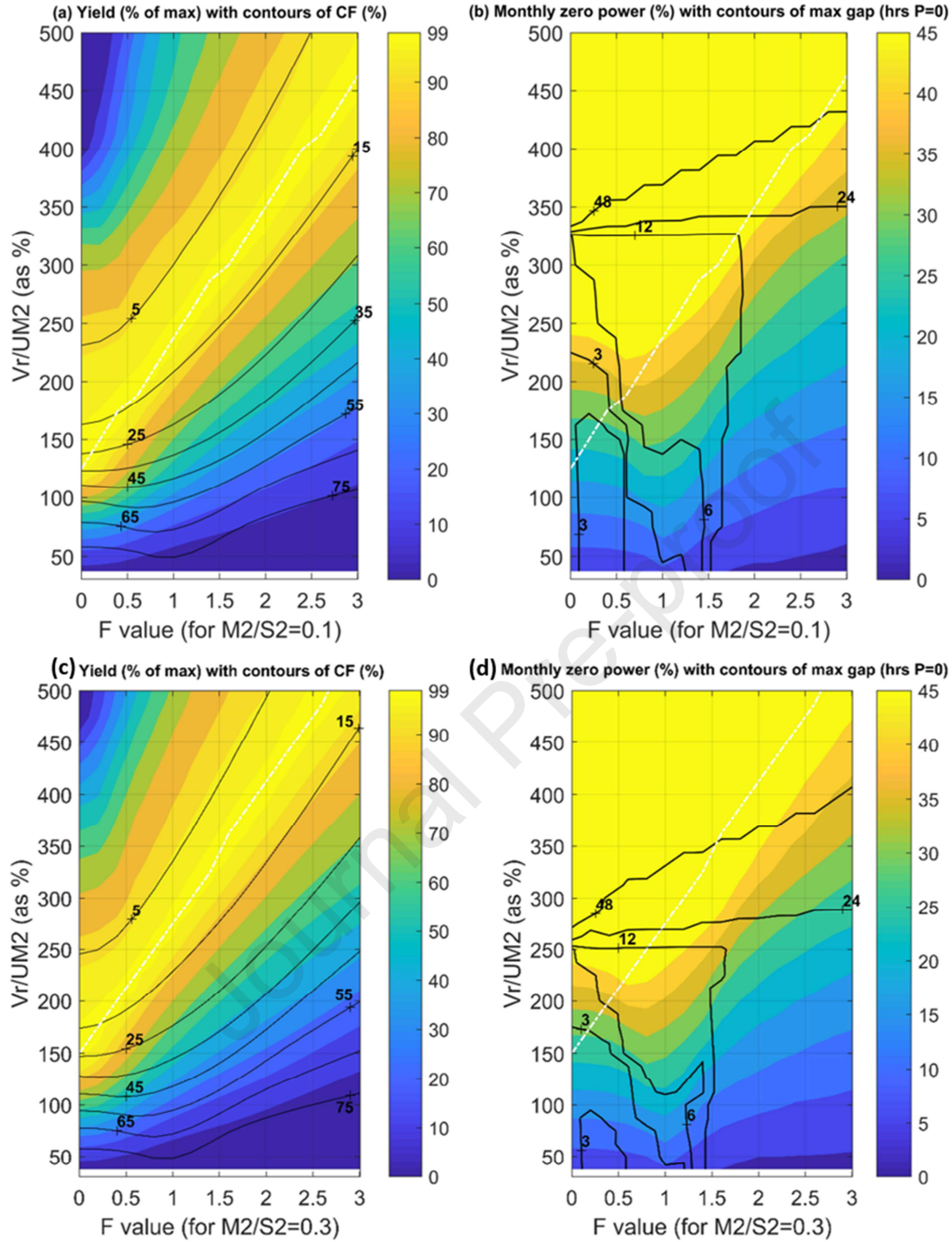807 **A2 (high yield density shown in blue) and Scenario B (firm power shown in red).**
808

809
810
811 **Appendix**
812
813

Fig A1. An example of sensitivity to the tidal-stream turbine optimisation result of Figure 7, when considering tidal dynamics with different M2/S2 ratios but equal F values. Tide currents harmonic characteristic tidal form (F value), rated turbine speed (relative to M2 current amplitude UM2) and subsequent yield and Capacity Factor (CF) shown in panel a and c; with mean monthly percentage of zero power and maximum period of no power (max gap) in panel b and d
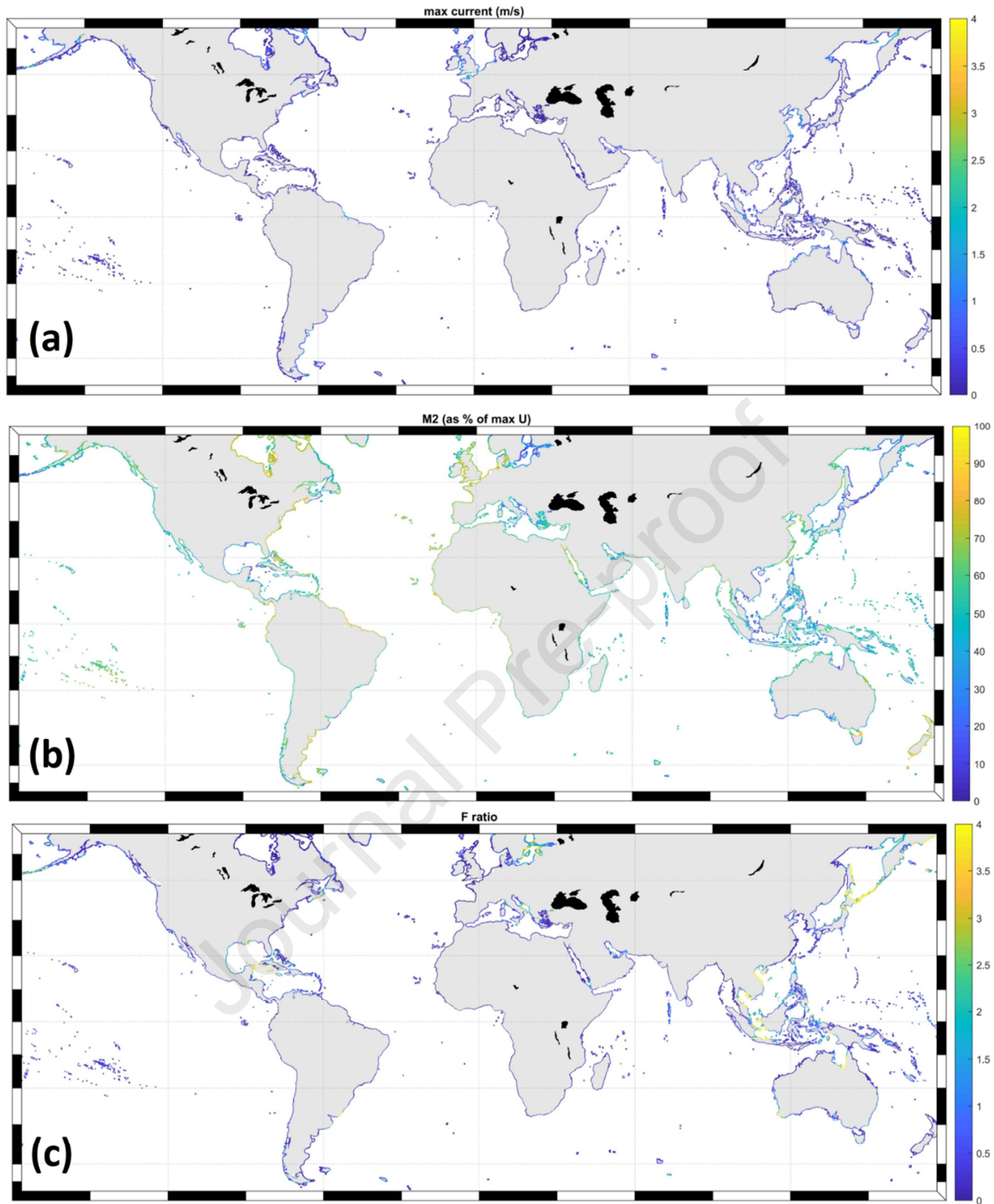
822
823
Fig A2. Global tidal dynamic variability, described as: (a) maximum current speed; (b)
percentage of M2 current amplitude compared to maximum current speed; and (c)
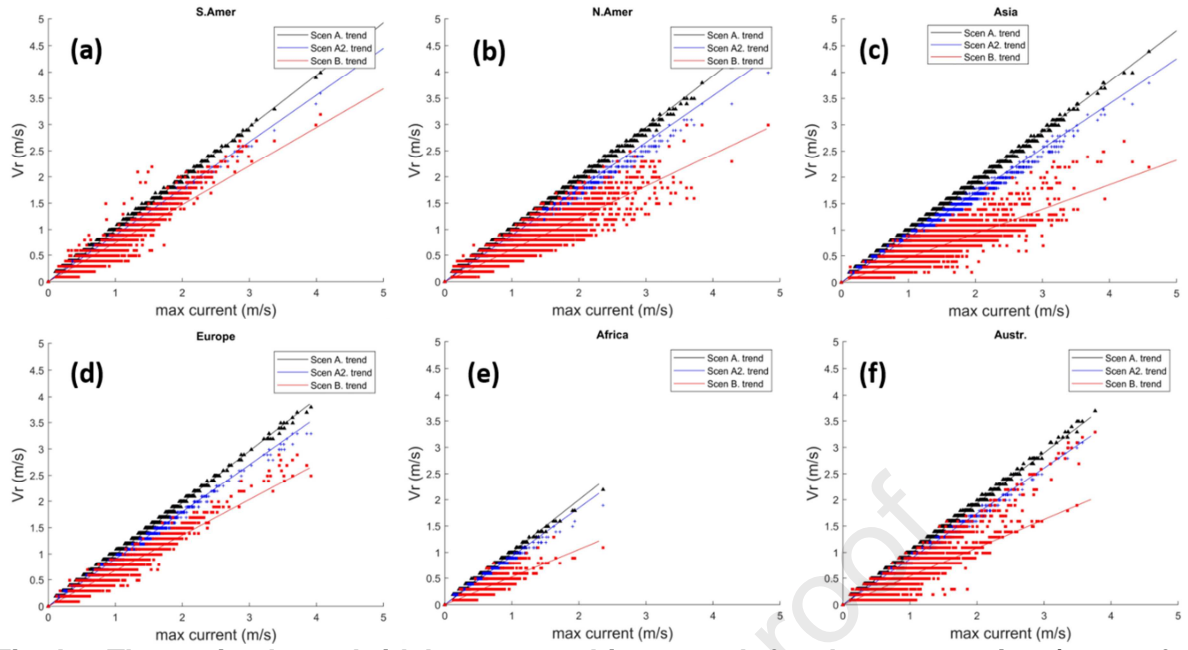**Tidal form (F-value) using FES2014 data**

827
828 **Fig A3. The optimal rated tidal-stream turbine speed, for three scenarios (a to c for**
829 **max, high and firm yield respectively), based on FES2014 global data and grouped**
830 **into the 6 continents: South America (a), North America (b), Asia (c), Europe (d),**
831 **Africa (e), Australasia (f).**
832
833

Table 1. A literature review of 14 horizontal axis tidal-stream turbines, where device characteristics are published or estimated (marked with *), including: rotor diameter (∅); Rated Power (Pr); power coefficient (C*p*); cut-in velocity (*Vs*) when the turbine starts to produce power; and rated velocity (*Vr*), the current speed when maximum power (*Pr*) is produced. Labels of devices in Fig. 2 are defined in the ID column.

ID	device	∅ (m)	*Pr* (kW)	*Vr* (m/s)	*Vs* (m/s)	*Vs* (as % of *Vr*)	*Cp**	source
1	**MCT**	16	600	*2.5*	*1*	40	0.37	Lewis et al. (2015)
2	**Alstrom**	18	1000	*2.7*	*1*	37	0.39	Lewis et al. (2019)
3	**sabella D-10**	10	1000	*4*	*1*	25	0.39	Website 1
4	**sabella D-15**	15	2300	*4*	*1*	25	0.4	Website 1
5	**seagen-S 2MW twin rotor**	20	1000 (per rotor)	*2.5*	*1*	40	0.4	Website 2
6	**Atlantis AR1000**	18	1000	*2.65*	---	---	0.41	Website 2; Roberts et al. (2016)
7	**Atlantis AR2000**	22	2000	*3.05*	*<1*	---	0.36	Encarnacion et al. (2019); Website 2
8	**Verdant gen5**	5	35	*2.59*	---	---	0.32	Polygae et al (2010); Encarnacion et al. (2019)
9	**Nova**	8.5	100	*2*	*0.5*	25	0.43	Encarnacion et al. (2019)
10	**Voith**	16	1000	*2.9*	---	---	0.4	Roberts et al. (2016)
11	**openhydro**	10	200	*2.5*	---	---	0.32	Polygae et al (2010); Roberts et al. (2016)
12	**schottel hydro d3**	3	70	*3.7*	*0.9*	24	0.38	Website 3
13	**schottel hydro d4**	4	62	*3.1*	*0.8*	26	0.32	Website 3
14	**schottel hydro d5**	5	54	*2.6*	*0.7*	27	0.31	Website 3
	Mean	**13**	**816**	*2.91*	*0.88*	*30%*	*0.37*	
	Standard Deviation	6	**803**	*0.6*	*0.18*	*7%*	*0.04*	

Table 2: Optimal rated tidal-stream turbine speed (*Vr*) relative to maximum tidal current speed (MaxU) at any given "coastal" site globally for three optimal power scenarios, with two methods of representing Vr: absolute with linear regression of max U and Vr (with linear regression score: RSQ), and Vr relative to maxU at site, discretised into 0.5m/s groups with mean Vr (as % maxU) and associated standard deviation (std), with the Pearson correlation score (RHO) is given to indicate strength of statistical fit at 5% confidence

		Optimal *Vr* scenario:		
		Max yield (scenario A)	High yield (scenario A2)	Firm power (scenario B)
Absolute *Vr* trend	RSQ	~100%	~100%	92%

trend	$Vr = 0.97*maxU$	$Vr = 0.87*maxU$	$Vr = 0.56*maxU$
maxU	Vr as % of maxU (std)		
0.5m/s	107 (17)	102 (17)	49 (13)
1.0m/s	99 (8)	93 (9)	48 (17)
1.5m/s	97 (4)	87 (4)	57 (16)
2.0m/s	96 (3)	86 (4)	59 (15)
2.5m/s	96 (2)	85 (4)	58 (16)
3.0m/s	96 (2)	84 (3)	58 (16)
3.5m/s	96 (2)	84 (3)	60 (17)
4.0m/s	96 (2)	85 (3)	64 (16)
4.5m/s	96 (2)	84 (3)	67 (12)
RHO	-0.28	-0.43	0.24

Mean Vr (as % of maxU) with standard deviation in brackets (std)

Table 3: The linear trend of optimal absolute rated turbine speed ("Trend" Vr in m/s), with each respective linear regression score (RSQ), for three tidal-stream energy scenarios (A , A2, and B) and spatially grouped data by continent, using four major tidal constituents of FES2014 data (latitude <70° and up to 25km offshore)

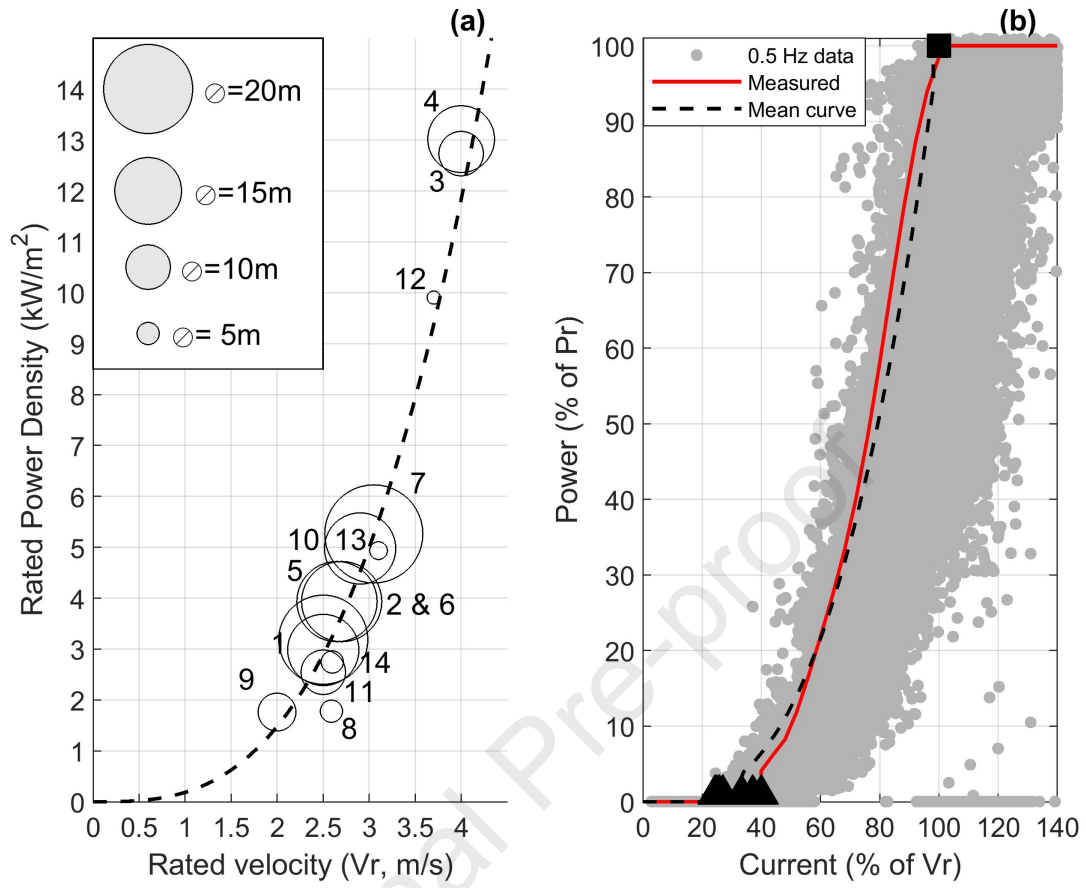| region	Scenario:	A (max yield)	A2 (high yield)	B (firm power)
World	RSQ	100%	100%	92%
	Trend	$Vr=0.97*maxU$	$Vr=0.87*maxU$	$Vr=0.56*maxU$
Europe:	RSQ	100%	100%	93%
	Trend	$Vr=0.96*maxU$	$Vr=0.85*maxU$	$Vr=0.46*maxU$
Australasia:	RSQ	100%	100%	91%
	Trend	$Vr=0.97*maxU$	$Vr=0.87*maxU$	$Vr=0.54*maxU$
Asia:	RSQ	100%	100%	93%
	Trend	$Vr=0.96*maxU$	$Vr=0.85*maxU$	$Vr=0.46*maxU$
Africa:	RSQ	99%	99%	91%
	Trend	$Vr=maxU$	$Vr=0.92*maxU$	$Vr=0.53*maxU$
North America:	RSQ	100%	99%	95%
	Trend	$Vr=0.98*maxU$	$Vr=0.89*maxU$	$Vr=0.61*maxU$
South America:	RSQ	100%	100%	96%
	Trend	$Vr=0.99*maxU$	$Vr=0.89*maxU$	$Vr=0.74*maxU$

Table 4: Comparison of optimal tidal-stream turbine rated speed (Vr) based on two scenarios (max yield and firm power; scenarios A and B respectively) using tidal harmonic data, giving peak current speed as the sum of the four major constituents (K1,O1,S2,M2), called maxU, as well as the amplitude of current speed for the M2 constituent (Ua), for high and coarse spatial resolution (Res.) model data comparison for the UK region. Comparison metrics: Root Mean Squared Error RMSE) and linear regression score (RSQ) provided alongside scatter and average conversion between resolutions.
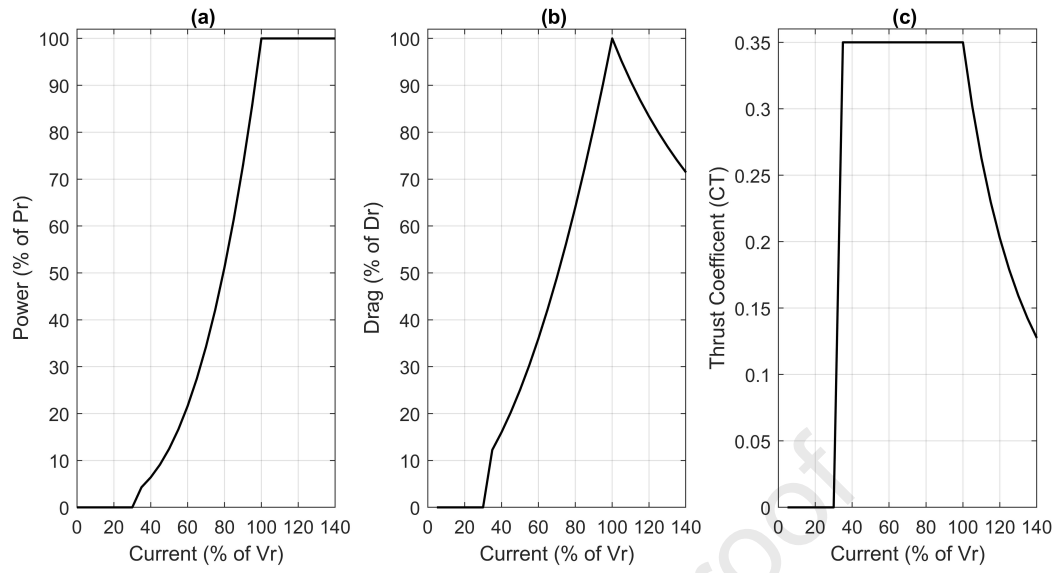
	High res. Robins et al. (2015) (~1km spatial	Coarse res. FES2014 (~7km resolution)

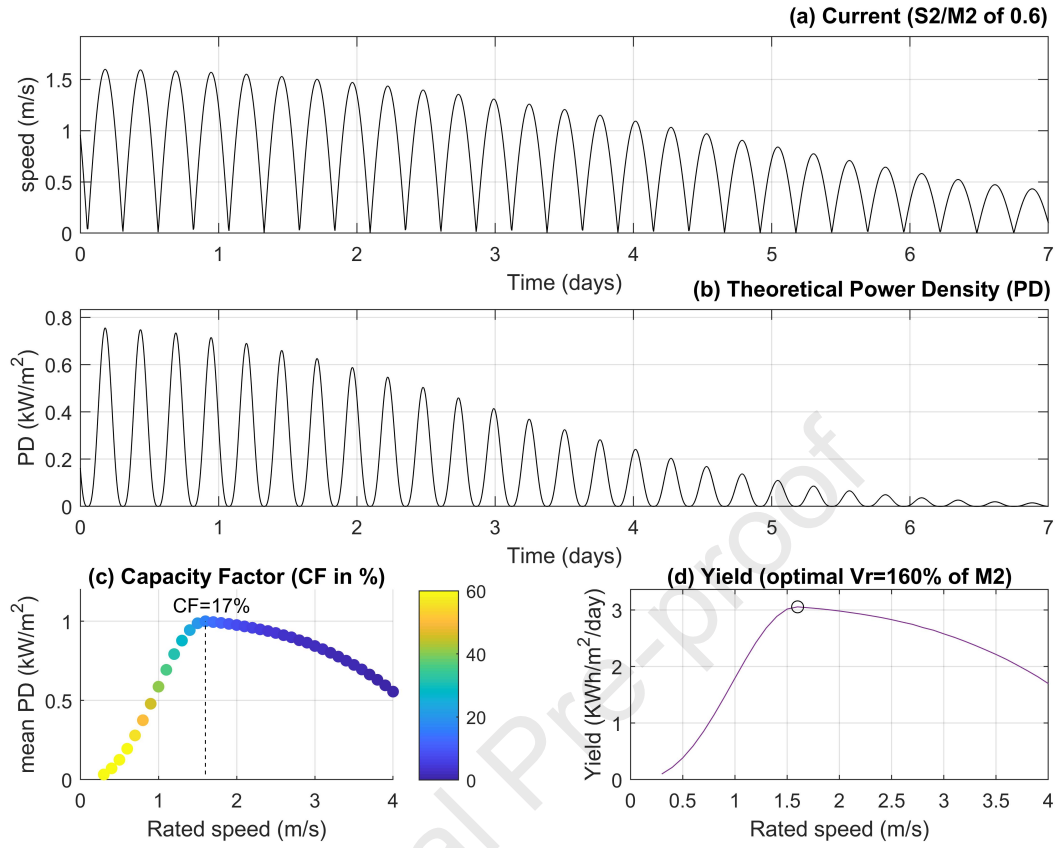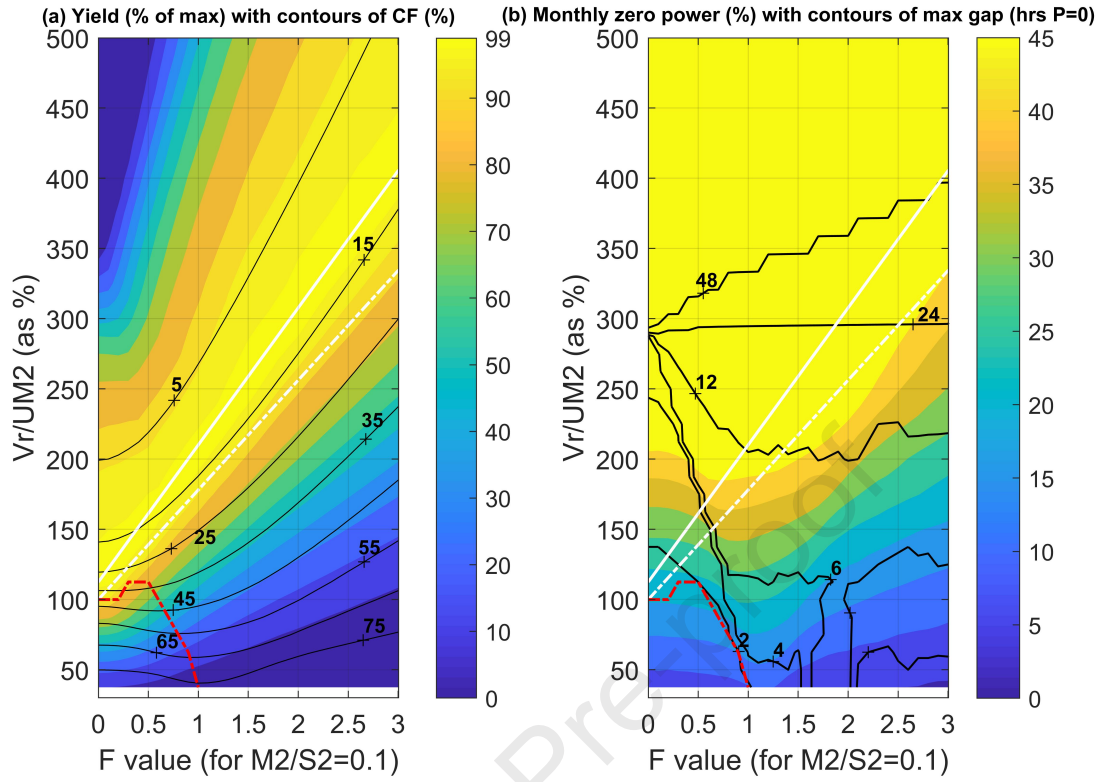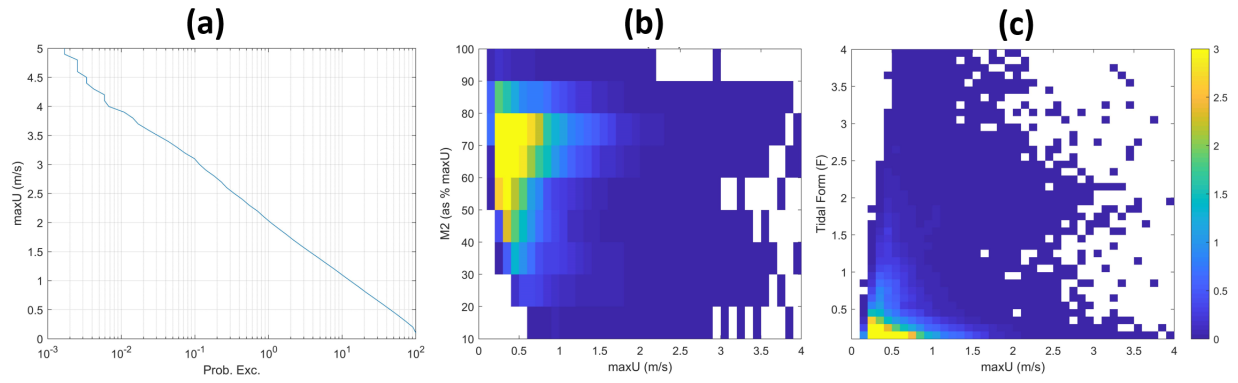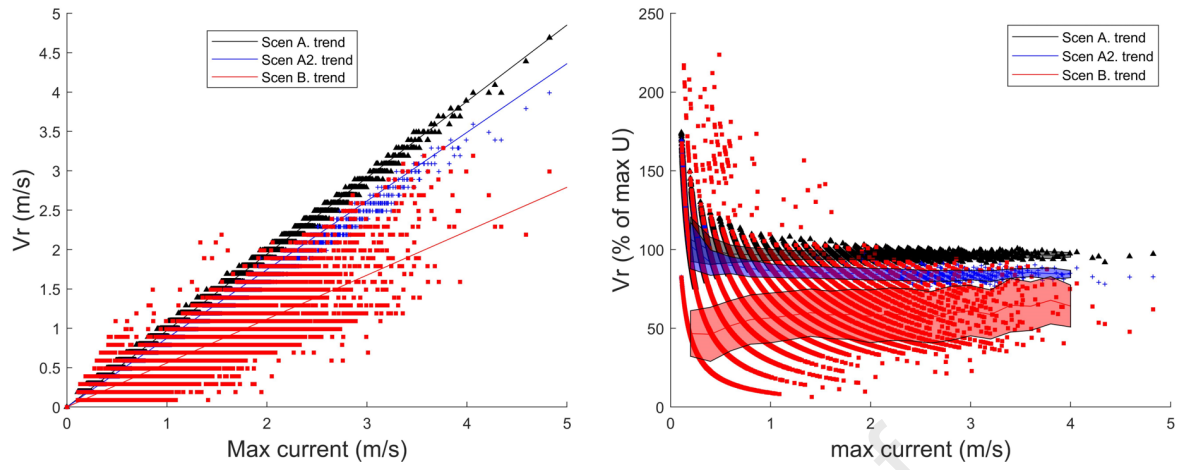|		
	resolution)	
Scenario A linear trend:	Vr~0.97maxU+0.01	Vr~0.98maxU
Scenario B linear trend:	Vr~0.58*maxU+0.05	Vr~0.56maxU + 0.27
M2 current amplitude comparison:	RMSE = 0.18 m/s (4%) RSQ = 71% Scatter Index = 31% Coarse(Ua) ~ 0.66*high(Ua)	
Maximum current comparison:	RMSE = 0.23 m/s (4%) RSQ = 71% Scatter Index = 28% Coarse res. (maxU) ~ 0.68*high res. (maxU)	

(a) Capacity Factor (CF)

(b) Time no power produced (%)

(c) Yield (% of max)

(d) Max. Time of no power (hrs)

(a) Tidal Current (M2=2m/s S2=1m/s)

(b) Theoretical Power Density (PD)

(c) Technical Power Density (PD)

mean power=0.71kw/m^2 (17.04kwh/m^2 per day), CF=25%, no power=36% (3.6hrs biggest gap)
mean power=0.58kw/m^2 (13.88kwh/m^2 per day), CF=39%, no power=17% (1.6hrs biggest gap)

(a) Current Speed

(b) Theoretical Power Density (PD)

(c) Capacity Factor (CF in %)

(d) Yield (optimal Vr=100% of M2)

(a) Current (S2/M2 of 0.6)

(b) Theoretical Power Density (PD)

(c) Capacity Factor (CF in %)

(d) Yield (optimal Vr=160% of M2)

(a) Yield (% of max) with contours of CF (%)   (b) Monthly zero power (%) with contours of max gap (hrs P=0)

(a)

(b)

(c)

Highlights:

- **Standardised horizontal-axis tidal-stream turbine power-density curve developed**
- **Convergent power curve characteristics assessed with global tide data**
- **Divergence in rated-speed when selecting for optimal yield or persistent power**
- **Resource-led turbine optimisation is possible but high resolution tidal data needed**
- **High and low flow designs appear needed to capitalise on resource predictability**